Dalton Transactions

ROYAL SOCIETY OF CHEMISTRY

PAPER

View Article Online
View Journal | View Issue

Cite this: *Dalton Trans.*, 2025, **54**, 7828

Quercetin and luteolin complexation with first-row transition metals in purely aqueous solutions: stoichiometry and binding site selectivity†

Giuseppina Anna Corrente, Luana Malacaria, Amerigo Beneduci, * Tiziana Marino and Emilia Furia

Received 26th February 2025,
Accepted 8th April 2025

DOI: 10.1039/d5dt00478k

rsc.li/dalton

The complexation behaviour of quercetin and luteolin with first-row transition metals (Cr(III), Mn(II), Co(II), Ni(II), and Zn(II)) in aqueous solutions was systematically investigated using potentiometric titrations, UV-Vis and FT-IR spectroscopy, and density functional theory (DFT) calculations. This study aimed to elucidate the stability, stoichiometry, and preferred binding sites of these flavonoid–metal complexes in an entirely aqueous solution at 37 °C as a function of pH under controlled ionic strength. Speciation analysis revealed the formation of 1 : 1, 1 : 2, and 1 : 3 metal-to-ligand complexes, with coordination occurring primarily at the 4,5- or 3,4-binding site, depending on the metal ion and ligand structure. UV-Vis and IR spectral changes confirmed complex formation, while computational modeling provided insights into binding site selectivity and free energy changes associated with coordination. Results highlight the influence of the ligand structure on metal affinity and stability, with quercetin forming more stable complexes than those formed by luteolin owing to the presence of an additional hydroxyl group at position 3. These findings contribute to a deeper understanding of flavonoid–metal interactions, with potential implications for antioxidant activity, metal chelation therapy, and environmental applications.

1 Introduction

Flavonoids are a ubiquitous class of secondary metabolites, belonging to one of the main groups of bioactive natural products,[1–3] comprising several thousand individual compounds. Their basic structural feature is the flavane (2-phenylbenzo-γ-pyrane) nucleus, a system of two benzene rings (A and B) linked *via* an oxygen-containing pyrane ring (C) (Scheme 1). According to the degree of oxidation of the C ring, the hydroxylation pattern of the nucleus, and the substituent at carbon 3, flavonoids can be categorized into the subclasses flavones, isoflavones, flavanols (catechins), flavonols, flavanones, anthocyanins, and proanthocyanidins.[1,2]

Flavonoids exhibit antioxidant activity through a combination of several mechanisms.[1,3] One of the most common and widely recognized is their free radical scavenging activity, arising from their direct reaction with free radicals, generating less reactive aromatic radical species (*i.e.*, ArO$^{\bullet}$ and ArOH$^{\bullet}$).[1–3] In addition, metal chelation was suggested as an alternative way to exert their protection against oxidative stress, a consequence of a chemical imbalance between production and consumption of oxidants within biological systems.[1,2] Indeed, Fenton-like reactions catalysed by some of the first row transition metals in their reduced form (*e.g.*, Fe(II) and Cu(II)) may occur, causing site specific accumulation of reactive oxygen species (ROS) and initiating biomolecule damage processes.[1,2] Metal-chelating compounds, such as flavonoids, can remove metals (either in the reduced or oxidized forms) from the catalytic cycle and/or the redox potentials of flavonoid chelating compounds can be altered, thus inactivating them and thereby behaving as an $^{\bullet}$OH-inactivating ligand (known as OIL).[2] Additionally, the antioxidant activity of flavonoids can be significantly increased through complexation with metals when coordination occurs at the 4,5 or 3,4 site, while leaving the 3′-OH and 4′-OH groups free, which are crucial for antioxidant activity.[2,4,5] Therefore, investigating the coordination sites of flavonoid complexes with various bioactive metals is of the utmost importance for understanding the potential antioxidant activity of these complexes and their prospective application as functional bioactive compounds.

Notably, each metal ion forms hydrated ions in water, which undergo pH- and concentration-dependent chemistry, which is influenced by the presence of metabolites, proteins and other biological components. It is important to recognize

Department of Chemistry and Chemical Technologies, University of Calabria, Via P. Bucci, Cubo 12D, 87036 Arcavacata di Rende (CS), Italy.
E-mail: amerigo.beneduci@unical.it

† Electronic supplementary information (ESI) available. See DOI: https://doi.org/10.1039/d5dt00478k

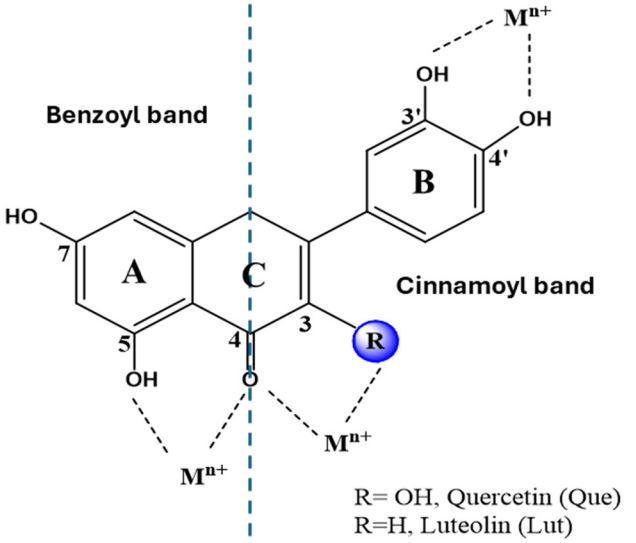

Scheme 1 Chemical structure of quercetin and luteolin. Metal binding sites considered. Structural moieties responsible for the main bands in the absorption spectra are evidenced (M = Mn, Co, Ni and Zn if n = 2; with n = 3 and M = Cr).

that redox active metal ions do not exist as free ions in cells[6,7] and could undergo speciation chemistry governed by the metal ion's oxidation state, ionic strength, pH and stability of the complexes between these cations and biological molecules.[6,7]

Another important rationale for studying the complexes formed by flavonoids with metals from the first-row transition series is their potential accumulation in the body, which can lead to human diseases. Although copper, cobalt, manganese, iron and zinc are essential to human health, and chromium, vanadium and nickel have shown some beneficial biological effects,[8–12] it is crucial that their levels remain within an acceptable range for normal function since excessive concentrations may result in toxicity while insufficient concentrations may result in nutritional deficiencies.[13,14] Diseases associated with excessive accumulation of essential and xenobiotic heavy metals (due to environmental pollution) in tissues can be treated using specific chelation targeting strategies[15–17]

Phenolic compounds also play a significant role in the metals' behaviour in plants through their mobilization from soil, translocation within the plant and their accumulation in specific tissues, the latter being the basis of phytoremediation.[18] Significantly, the concept of "metallophenolomics" has emerged as a subset of metallomics, focusing on ligand-oriented studies of phenolics–metal(loid) complexations. This integrated approach offers insight into the interactions between phenolics and metal(loid)s in biological systems.[18]

Therefore, studying phenolic compounds as exogenous (animals) and endogenous (plants) complexing agents of metals from the first row series is crucial for biological systems.

In addition, most of those metals (such as Cu, Zn, Co, and Ni) are main components of electrical/electronic wastes and should be recovered to prevent environmental pollution[19,20] and enable their reuse as secondary raw materials.[21] Hence, developing systems based on natural chelators for selective removal of heavy metals from environmental matrices and selective recovery of precious metals from e-wastes is crucial for environmental sustainability and resource efficiency.

Finally, flavonoids are promising coordination materials for the development of functional molecular architectures for nanotechnology applications. A rational design of these nanomaterials is based on a clear comprehension of the coordination behaviour of phenolic ligands with the stabilizing metals (*e.g.*, Fe and Zn), which drives the self-assembly of supramolecular metal–phenolic networks.[22,23]

For the first time, we systematically investigated the complexation behaviour of quercetin and luteolin model flavonoids with specific first-row transition metals in an entirely aqueous medium. This is particularly significant because both ligands have sparingly water solubility, and previous studies on their metal complexation, including with first-row transition metals, were conducted in organic or mixed water/organic solvents.[22,24–32] However, those studies do not provide definitive conclusions regarding the stoichiometry and binding sites involved in metal–flavonoid coordination. In addition, complex formation in water may differ significantly from that in organic solvents, particularly when key experimental parameters such as pH, ionic strength, temperature, and metal/ligand mole ratio are not strictly controlled. In our recent research, we reported data on the complexation of quercetin with Al(III), Fe(III) and Cu(II)[33] and quercetin and luteolin with Al(III) and first-row transition metals in aqueous media.[33,34] However, the results were not entirely consistent for quercetin regarding the pH range of complex formation, complex stoichiometry, and binding sites involved, likely due to differences in the experimental conditions. Therefore, a systematic investigation of both flavonoids' complexation behaviour with first-row transition metals in a purely aqueous environment under well-controlled experimental conditions is essential. In this study, we designed an experimental setup that ensured the controlled interaction of metals with a saturated aqueous solution of the ligand, maintaining consistent ionic strength and temperature. Complexes formation was then monitored potentiometrically as a function of pH upon addition of a known amount of strong base. The selected metals were Cr(III), Mn(II), Co(II), Ni(II) and Zn(II). Quercetin (H_5Que) served as a model ligand due to its three different coordination sites, illustrated in Scheme 1 (with R = OH): the 3′,4′-*ortho*-dihydroxyl site of the ring B (catechol binding site), the 5-hydroxy-4-keto group on the ring A (acetylacetone binding site), and the 3-hydroxy-4-keto group on ring C (3-hydroxychromone binding site). Luteolin (H_4Lut) was chosen as it lacks the 3,4 binding site, as depicted in Scheme 1 (R = H). The comparative study of both model compounds is expected to shed light on possible interferences of the different sites in selective binding.

Assignment of the metal coordination site in ligands that offer different binding positions is not straightforward, often requiring a combination of various characterization

techniques.[4,32] To achieve this, we utilized UV-Vis and FT-IR spectroscopic techniques complemented by density functional theory (DFT) calculations to distinguish between the various binding sites. The data obtained from UV-Vis and FT-IR spectral analysis combined with the insights from DFT calculations, enabled the identification of the most likely complexes in solution, regardless of the ligand/metal ion stoichiometric ratio. These findings allowed us to derive some general conclusions about the characteristics of the complexes formed by both ligands with the investigated cations.

2 Experimental

2.1 Materials

Sodium perchlorate, perchloric acid and sodium hydroxide titrant solutions were prepared and standardized as previously described.[35] Chromium(III), manganese(II), cobalt(II), nickel(II) and zinc(II) perchlorate stock solutions were prepared and standardized as reported previously.[35–39] Quercetin (Sigma, ≥95%) was kept in a desiccator over silica gel and was used without further purification; luteolin (Sigma, ≥98%) was kept at 4 °C and used without further purification. All solutions were freshly prepared with double distilled water.

2.2. Potentiometric measurements

The complex formation equilibria between quercetin and luteolin and the investigated metal ions, *i.e.*, Cr(III), Mn(II), Co(II), Ni(II) and Zn(II), generically M, were studied by performing potentiometric titrations with cell (G) and measuring the competition of the ligand for the metal cations and H^+ with a glass electrode, GE, at 37 °C and in 0.16 M $NaClO_4$:

$$\text{RE/test solution/GE} \quad \text{(G)}$$

where, the reference electrode, RE = Ag/AgCl/0.01 M NaCl/(0.16–0.01) M $NaClO_4$/0.16 M $NaClO_4$ and test solution = C_M M $M(ClO_4)_n$, C_A M $HClO_4$, C_B M NaOH, $(0.16 - nC_M - C_A - C_B)$ M $NaClO_4$. This background salt was chosen to control the ionic strength due to its high inertia towards complexation and was preferred to NaCl, which it is not suitable for many metals that belong to the borderline category. Moreover, it is possible to prepare solutions with a high degree of purity in the case of $NaClO_4$. The metal (C_M) concentration ranged from 0.1 to 5.0 mM. Each metal was put in contact with a saturated solution of each ligand. Due to their very low solubility in water, the metal-to-ligand ratio was controlled by the metal concentration. Given the solubility values of approximately 0.1 mM for quercetin[40] and 0.01 mM for luteolin,[41] the estimated metal-to-ligand mole ratio ranges from 1 : 1 to 50 : 1 for quercetin and from 10 : 1 to 500 : 1 for luteolin. The hydrogen ion concentration was varied from 10 mM (pH 2.0) to incipient precipitation of a neutral species, which takes place in the range $[H^+] = 0.1 \times 10^{-3}$–$3.2 \times 10^{-8}$ M (pH 4.0–7.5), depending on the specific metal ion and on the metal-to-ligand ratio investigated. A constant potential within 0.1 mV was measured using the glass electrode (Metrohm) 40–50 min after the addition of the reagents. The EMF of the cell (G) can be deduced in mV at 37 °C using eqn (1):

$$E = E_0 + 61.54\log[H^+] + E_j \quad (1)$$

where E_0 is constant in each series of measurements and E_j is the liquid junction potential taken from literature,[39] which is a function of $[H^+]$ only.[42] In the first part of each titration, E_0 was determined in the absence of metal cations and ligand. In detail, the acidity of the test solution (*i.e.*, 20 mL 0.16 M $NaClO_4$) was varied by adding gradually 2.5 mL of 10 mM $HClO_4$ titrant solution. In the $[H^+]$ range 10^{-4}–10^{-2} M constant values were calculated in the range from 310 to 350 mV to within 0.1 mV. In the second part, the acidity was decreased stepwise by adding NaOH standard solution using a manual burette. The titrant's concentration varied from 5.0 to 25.0 mM and the final titrant volume was from 10 to 50 mL, depending on the specific metal-to-ligand ratio investigated. To avoid carbonate interference, a slow stream of nitrogen gas was passed into the test solutions and stirred magnetically. The cell assembly was placed in a thermostat kept at 37.0 ± 0.1 °C.

The formation constants were determined using a least-squares fitting of the potentiometric data with SUPERQUAD.[43] Additionally, the experimental results were analysed using a graphical approach, which involves comparing the potentiometric data with model functions.[44] It was initially assumed that the primary reaction products were binary complexes with mononuclear metal ions. This assumption was tested by plotting Z, the average number of ligands per metal ion, against pH. If ML-type complexes dominated, the experimental data points collected at various ligand and metal concentrations would align with a single theoretical curve. However, additional complexes were proposed when systematic deviations from this simple binary model were observed and their stoichiometry was determined using numerical analysis.

2.3 FT-IR and UV-Vis characterization

FT-IR spectra were acquired with a Shimadzu IR Affinity-1S spectrometer (Shimadzu Corporation) in the spectral region of 375 and 4000 cm^{-1} with a resolution of 1 cm^{-1}, 64 scans for a single analysis and using KBr pellets. The KBr pellets were obtained by mixing the solid sample collected at the end of the potentiometric titration with KBr powder (ratio 1 : 200) and pressing with a hydraulic press at the pressure of 6 tons for 5 minutes. The resulting pellets were placed in the appropriate compartment of the instrument and exposed to the FT-IR light beam for analysis. UV-Vis spectra were recorded using a Jasco V-550 UV-Vis spectrophotometer on samples arising from the solution or the solid precipitates collected at the end of the titration. The solutions were filtered using a 0.45 μm filter prior to spectral acquisition, while the solids were washed with water and dissolved in ethanol. Spectrophotometric measurements were carried out by measuring the absorbance values, A_λ, (to 0.001 units) between 200 and 650 nm each 1 nm. Measurements were performed at 25 °C.

Deconvolution analysis of the UV-Vis absorption spectra was performed by using the Gauss model expressed by eqn (2):

$$y = y_0 + \frac{A}{w\sqrt{\pi/2}} e^{-2\left(\frac{x-x_c}{w}\right)^2} \quad (2)$$

where, y_0 is the offset, A = area, x_c = centre, $w = \frac{\mathrm{FWHM}}{\sqrt{\ln 4}}$

2.4 Plots and fitting

All plots and the fitting procedures were performed using Microsoft Excel and Origin Versions 2019b and 2022b (OriginLab Corporation, Northampton, MA, USA).

2.5 Computational methods

All the DFT computations were carried out using the Gaussian16 code.[45] The geometry optimizations, without any symmetry constraint. All the considered species were done in solution by employing the Minnesota M052X exchange-correlation functional coupled with the 6-31+G(d) basis set for C, H, and O atoms except for Cr, Mn, Co, Cu and Zn atoms, for which the relativistic compact Stuttgart/Dresden effective core potential was used in conjunction with its split valence basis set. Solvent effects were considered by using the solvation model based on density (SMD),[46,47] and a dielectric constant of 78.0 was used for water. The SMD continuum model was chosen for simulating the solvent considering previous evidence suggesting that it is suitable for charged or non-charged solutes in quite diverse solvents or liquid media.[45] It was also proved to be appropriate for mixed models, geometry optimization, and vibrational calculations in solution.[46] Vibrational analysis was performed at the same level of theory to evaluate the nature of the stationary point of the optimized systems and zero-point vibrational corrections were added to the electronic energies. Metal binding affinity of Que and Lut to Cr(III), Mn(II), Ni(II), Co(II) and Zn(II) was evaluated, as previously reported,[32] considering the following reaction (eqn (3)):

$$\{nL\}^c + [M(H_2O)_6]^z \rightarrow [ML_n]^{z+c} + (6-n)H_2O \quad (3)$$

where c is the total formal charge of the ligand; L = ligand (Que or Lut), OH^-; z is the charge of the hexaaquo complex, only considering that the ligand is bidentate. The reaction free energies in the general complexation reaction for the substitution of water molecules in the hexaaquo complex were calculated using eqn (4):

$$\Delta G_f = \Delta G\left([ML_n]^{z+c}\right) + (6-n)\,\Delta G\,(H_2O) - \Delta G\left(\sum_i^n (L_i)^c\right) - \Delta G\left(\left[M(H_2O)_6\right]^z\right) \quad (4)$$

NBO analysis and electrostatic potential calculations were performed using Gaussian16 code.[45] Preliminary calculations were performed for Zn(II), Co(II), Ni(II), Cr(III) and Mn(II) ions using unrestricted Kohn–Sham (UKS) calculations to establish the most stable spin multiplicity, which helps verify the absence of spin contamination. These computations clearly indicate the favored spin state: quartet for Cr, sextet for Mn, quartet for Co, triplet for Ni and singlet for zinc complexes.

Time dependent (TD) extension of DFT was used to calculate vertical excitation energies for the first 40 singlet excited states to simulate the UV-Visible spectra of free and complexed ligands. The analysis of the electronic structure and spectra of molecules was performed by Chemissian.[48]

3 Results and discussion

3.1 Potentiometric results

The experimental data were explained according to the general equilibria (eqn (5) and (6)):

$$pM^{n+} + rH_5Que \rightleftarrows M_p(H)_{-q}(H_5Que)_r^{(np+q)} + qH^+ \quad (5)$$

$$pM^{n+} + rH_4Lut \rightleftarrows M_p(H)_{-q}(H_4Lut)_r^{(np+q)} + qH^+ \quad (6)$$

in which the stoichiometric coefficients p, q and r are referred to the metal ion, proton and ligand, respectively. These equilibria consider all the possible complexes formed in solution and all the potential chelation sites of quercetin and luteolin, which correspond to a different number of protons involved in the formation of the complexes. The potentiometric data were analysed graphically and numerically to determine the stoichiometric coefficients of the complexes and their corresponding stability constants ($\beta_{p,q,r}$) (Table 1). This analysis enabled the construction of the distribution diagrams shown in Fig. S1.† The potentiometric results clearly show that both ligands form complexes at 1 : 1, 1 : 2 and 1 : 3 cation-to-ligand ratios with the metal cations considered. Interestingly, each metal can form more than one complex with different stoichiometry in most of the cases using a wide pH range and in the metal-to-ligand ratios investigated.

3.2 DFT analysis

The binding selectivity between the metal ions and the ligands was predicted using density functional theory (DFT) calculations[33,49,50] with r set to 1 in eqn (5) and (6) (Table 1). Complex formation was assumed to occur through substitution reactions of aquo metal complexes of the metal ions, proceeding *via* the loss of H_2O molecules. Free energy changes in the general complexation reaction for substituting water molecules in the hexaaquo complex were calculated, drawing from previous studies involving other metal ions[22,51] and will be discussed below. All the starting geometries were assumed to be octahedral with water molecules occupying the coordination sites that the ligand had left vacant. In addition, only the capability of the ligand to act as bidentate ligand was explored. Based on the observed loss of protons determined in the potentiometric analysis (Table 1), the complexes of quercetin with stoichiometry (1, 1, 1) can only form upon deprotonation of the ligand to the H_4Que-species. This holds for Cr, Co, and Zn (Table 1). Thermodynamically, the six-membered chelate ring formed upon coordination with the metal ion at

Table 1 Stoichiometries, stability constants and corresponding binding site selectivity of the complexes between quercetin and luteolin with Cr(III), Mn(II), Co(II), Ni(II) and Zn(II) in the pH range reported, according to equilibria (5) and (6)

					Site selectivity[a] (%)		
Metal ion	pH	(p,q,r)	Species	$\log \beta_{p,q,r} \pm 3\sigma$	4,5[c]	3,4[d]	3′,4′[e]
Ligand: H_5Que							
Cr(III)	2–5	(1,1,1)	$Cr(H_4Que)^{2+}$	−0.16 ± 0.09	81	19	
		(1,2,2)	$Cr(H_4Que)_2^{+}$	−9.6 ± 0.2			
		(1,3,1)	$Cr(OH)_2(H_4Que)$	−2.5 ± 0.3	9	91	
		(1,3,2)	$Cr(OH)(H_4Que)_2$	−7.2 ± 0.2			
Mn(II)	2–7	(1,2,1)	$Mn(OH)(H_4Que)$	−9.1 ± 0.3	32	68	
[b]Fe(III)	2–5	(1,4,1)	$Fe(OH)_2(H_3Que)^-$	−6.98 ± 0.06			100
Co(II)	2–5	(1,1,1)	$Co(H_4Que)^+$	−4.54 ± 0.09	84	16	
		(1,2,2)	$Co(H_4Que)_2$	−7.3 ± 0.3			
		(1,3,3)	$Co(H_4Que)_3^-$	−10.1 ± 0.3			
Ni(II)	2–7	(1,2,1)	$Ni(OH)(H_4Que)$	−11.70 ± 0.03	1	99	
[b]Cu(II)	4–7	(1,1,1)	$Cu(H_4Que)^+$	−3.12 ± 0.03	96	4	
Zn(II)	2–7	(1,1,1)	$Zn(H_4Que)^+$	−5.34 ± 0.09	19	81	
		(1,2,2)	$Zn(H_4Que)_2$	−9.38 ± 0.06			
Ligand: H_4Lut							
Cr(III)	2–5	(1,1,1)	$Cr(H_3Lut)^{2+}$	−1.4 ± 0.2	100		
		(1,3,1)	$Cr(OH)_2(H_3Lut)$	−9.58 ± 0.09	100		
Mn(II)	2–7	(1,1,1)	$Mn(H_3Lut)^+$	−4.43 ± 0.06	89		11
Co(II)	2–7	(1,1,1)	$Co(H_3Lut)^+$	−4.86 ± 0.06	99		1
		(1,2,1)	$Co(OH)(H_3Lut)$	−12.4 ± 0.3	100		
Ni(II)	2–6	(1,2,1)	$Ni(OH)(H_3Lut)$	−3.10 ± 0.09	100		
		(1,3,2)	$Ni(OH)(H_3Lut)_2^-$	−5.4 ± 0.2			
		(1,3,3)	$Ni(H_3Lut)_3^-$	−2.5 ± 0.3			
Zn(II)	2–7	(1,2,1)	$Zn(OH)(H_3Lut)$	−4.4 ± 0.1	100		
		(1,3,2)	$ZnOH(H_3Lut)_{2-}$	−5.1 ± 0.2			

[a] Calculated considering the Boltzmann distribution of binding states at 37 °C using the following equation: $\text{Site selectivity} = \frac{e^{-\Delta G_j/k_B T}}{\sum_1^n e^{-\Delta G_i/k_B T}}$ where, ΔG_j is the Giggs free energy of formation of the complex at the specific site j and the sum at the denominator is done across all the three possible sites all the possible sites with $n = 2$ and 3 for Lut and Que, respectively. [b] From ref. 25. [c] 4,5 site = 5-hydroxy-4-keto (acetylacetone). [d] 3-Hydroxy-4-keto (3-hydroxychromone). [e] 3′,4′-*ortho*-Dihydroxyl (catechol).

the 4,5 site is the most stable for Cr and Co complexes, as indicated by the calculated formation free energies (Table S1†) and binding site selectivity of about 80% (Table 1).

These two metals align with the behaviour of Cu(II) which has a high binding selectivity for the acetylacetone site (Tables 1 and S1†).[33] In contrast, the five-membered ring at the 3,4 site is preferred by Zn (Fig. 1a, Table S1 and Fig. S2†), with a selectivity of 81% (Table 1).

Speciation analysis suggests different stoichiometries for the complexes of manganese and nickel (1,2,1), arising from the overall loss of two protons (Table 1). Thus, the two scenarios are: (a) the ligand loses both protons at the catechol moiety ($M(H_3Que)$); (b) one of the two protons originates from a water molecule in addition to the ligand ($M(OH)(H_4Que)$). Specifically, the most likely species are $Mn(OH)(H_4Que)$ and $Ni(OH)(H_4Que)$ from the free energy changes associated with the complexation reaction (Table 1), with their optimized geometries shown in Fig. 1a. The $M(H_3Que)$ stoichiometry (Fig. S2†) is less favourable, with the free energy of complexation about 7 kcal mol^{-1} less negative for nickel and 4 kcal mol^{-1} less negative for manganese. For both metal ions, theoretical calculations for the hydrolysed species $Mn(OH)(H_4Que)$ and $Ni(OH)(H_4Que)$ indicate complexation at both the 3,4 and 4,5 sites (Table S1†), with the 4,5-conformation only 2.7 kcal mol^{-1} higher than the 3,4-conformation for nickel and only about 0.6 kcal mol^{-1} higher for manganese, with corresponding binding site selectivity for the 3,4 site of 99% and 64%, respectively (Table 1). The selectivity for the catechol site is close to zero for all the complexes, although the complexes at this site show relatively high negative Gibbs free energy for binding (Table S1†). In the first-row transition metal series, Fe(III) is the only metal that binds to the catechol site of Que in water, forming the stable, negatively charged complex $Fe(OH)_2(H_3Que)^-$ (Table 1 and Table S1†).[33]

Luteolin exhibits coordinating behaviour very similar to quercetin. Except for zinc, all complexes exhibit octahedral coordination geometry, consistent with the quercetin complexes. Since the deprotonated species H_3Lut^- is the only one involved in complex formation (Table 1), it was exclusively considered in the calculations. In general, the most stable configuration features H_3Lut^- coordinating through the 4,5 site among the complexes investigated for Cr, Mn, and Co, with binding selectivity larger than 89% (Table 1 and Table S1†), resulting in the formation of a six-membered chelate ring (Fig. 1b and Fig. S3†). The Gibbs free energy values of formation for luteolin complexes suggest a reduced metal ion affinity across all metal ions (Table S1†), likely due to the ligand's lower nucleophilicity owing to the absence of the OH moiety on ring C.

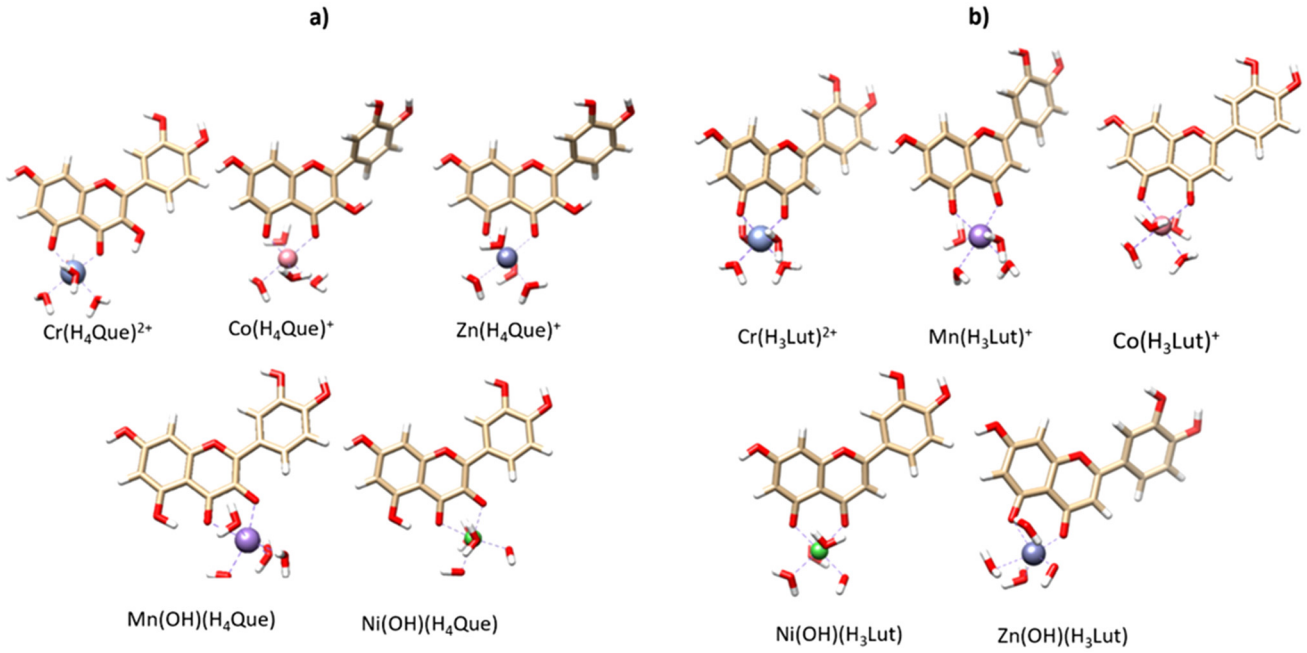

Fig. 1 Optimized structures for the most plausible complexes of (a) Que and (b) Lut with Cr(III), Mn(II), Ni(II), Co(II) and Zn(II).

For manganese, the coordination is primarily electrostatic, as evidenced by minimal electronic charge transfer between the metal and the ligand. This is supported by the NBO charge values, which remain close to those of the free ligand (Table S2†), consistent with manganese's hard-ion nature. In contrast, despite the total charge of the complex of chromium with H_3Lut^- being +2, it generates relatively weak electrostatic interactions, with a charge of 1.191|*e*|, compared to 1.425|*e*| for manganese and 1.263|*e*| for cobalt. For nickel and zinc, the species Ni(OH)(H_3Lut) and Zn(OH)(H_3Lut) (Fig. 2b) are the most energetically favourable configurations (Table S1†) with a selectivity of 100% for the acetylacetone site (Table 1). The nickel species Ni(OH)(H_3Lut) has an octahedral coordination geometry in its high-spin state (in contrast to the square planar geometry typically preferred for low-spin nickel complexes).

In the case of zinc, a water molecule in the apical position shifts to the second coordination shell (at a distance from the metal centre of 2.323 Å *vs.* 2.134 Å of the water coordinated to Zn), to minimize repulsions, resulting in a tetrahedral-like geometry. This behaviour reflects the chemistry of zinc which enables it to differentiate between quercetin and luteolin ligands, despite its borderline acid nature. Under identical experimental conditions, the absence of the OH group on luteolin's ring C leads to the deprotonation of an aqua ligand, forming Zn(OH)(H_3Lut). NBO charges suggest that the interaction is primarily electrostatic in nature (1.464|*e*|), with a binding energy of 34.5 kcal mol^{-1}, approximately 20 kcal mol^{-1} greater than that for quercetin (Table S2†).

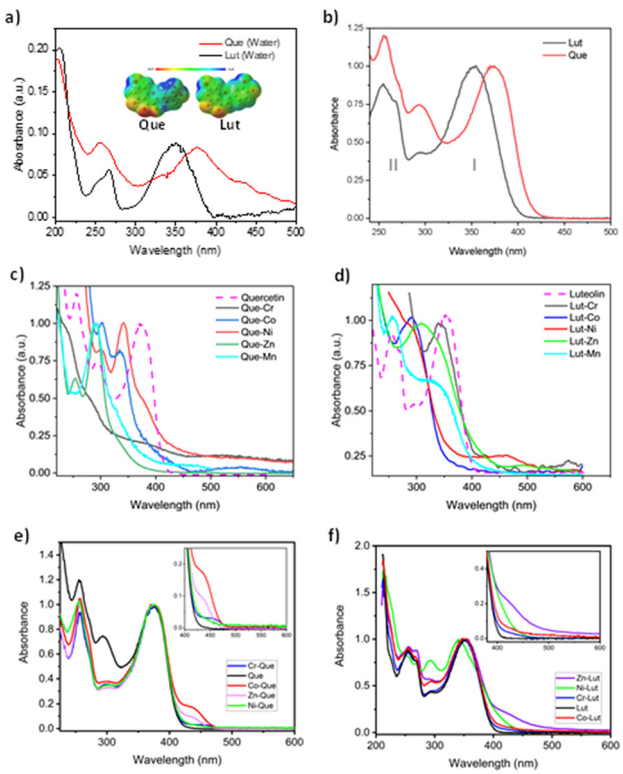

Fig. 2 UV-Vis spectra of the free ligands acquired from (a) saturated aqueous solutions and (b) in ethanol solutions. The inset in (a) contain the electrostatic potential maps (MEP) of the free ligands. (c) and (d) UV-Vis spectra of the solutions of Que and Lut with different metal cations, sampled at the end of the potentiometric titrations, (e) and (f) UV-Vis spectra of the solutions obtained by dissolving the solid precipitates collected at the end of the titrations in ethanol.

By comparing those species with the same stoichiometry and structure, there is an almost decreasing trend in the stability of the complexes moving along the first row of transition metal series. The stability follows the order Cr > Ni > Mn > Cu > Co ~ Zn for quercetin complexes with MH_4Que^+ stoichiometry (Table S1†). For luteolin complexes the theoretical affinity values follows the order Cr > Co ≈ Mn, with chromium exhibiting a significantly higher binding affinity (Table S1†). In contrast, the stability of the complexes is comparable in species in which a hydroxide is in the coordination sphere of the metal ions (Table S1†). Moreover, except for zinc, quercetin complexes are more stable than the analogous with luteolin, underlining the higher sequestering ability of quercetin towards the investigated metal ions compared with luteolin.

3.3 UV-Vis spectroscopy

The UV-Vis spectra of Que and Lut solutions in pure water (Fig. 2a) and in ethanol (Fig. 2b) show similar spectral features, although those acquired in saturated aqueous solutions have very low intensity due to the scarce solubility of the flavonoids in water. The two main absorptions of both ligands have already been largely characterized:[33,49] the cinnamoyl band (I) (~300–380 nm) is attributed to the S_1 state, mainly involving a HOMO → LUMO transition with both orbitals largely delocalized across the conjugated backbone (A + B and C fragments), although the largest linear combination of atomic orbitals LCAO is in the B and C rings.[49] The benzoyl band (II) (~240–300 nm) is mainly described by a HOMO → LUMO+1 transition with a significant intramolecular charge transfer character, and is attributed to ring A due to the largest LCAO contribution in this ring (Fig. 2a).[49]

The spectrum of Que is red-shifted with respect to that of Lut, especially the absorption band (I) (Fig. 2). Consistently, the simulated UV-Vis spectra of the free neutral ligands reported in Fig. S4† show this bathochromic shift attributed to the electron-withdrawing effect of the OH group in position 3 of Que, which increases the electron delocalization in the B ring, as supported by the electrostatic potential maps (MEP) reported in the inset in Fig. 2a. Generally, the increase in π-conjugation due to the 3-OH group in flavonols with respect to flavones leads to a bathochromic shift.[49]

The experimental UV-Vis spectra of both ligands can be well deconvoluted by the superposition of four/three bands for Que and Lut, respectively (Fig. S4†) with the λ_{max} reported in Table 3 and Tables S3–S6.†

The formation of complexes was examined by obtaining UV-Vis spectra of both the filtered solutions (Fig. 2c and d) and the solid material (Fig. 2e and f) collected after the potentiometric titrations and by DFT spectral simulations. Depending on the metal cation, the speciation in solution can be quite complicated, as illustrated in Table 1 and in the speciation diagrams in Fig. S1.† Therefore, the spectroscopic analysis of both the solutions and the precipitates can offer a more realistic snapshot of the systems at the highest attainable pH value during titration. The formation of complexes can be detected through shifts and/or the formation/disappearance of certain bands, reflecting the structure of the complexes. To this aim, the spectral deconvolution analysis (Fig. S5, S6 and Tables S7–S10†) provided quantitative insights into the spectral changes induced by complexation. This analysis helped in determining the wavelength shift and the relative contribution of each band to the overall spectrum compared to the free ligands, aiding in the discrimination of the binding sites involved. Table 2 presents the UV-Vis spectral data comparing the free ligands with solutions sampled at the end of the potentiometric titrations with the different metal cations. For quercetin, key features in all complex-associated spectra include: (i) a notable alteration in band (I) characterized by the bleaching of the component at 380 nm and a blue shift (>20 nm) of that at 345 nm, and (ii) the appearance of a new

Table 2 UV-Vis spectral data for quercetin, luteolin and the corresponding complexes formed in aqueous solution during potentiometric titration

			Band II		Band I		Bands associated with soluble complexes		Bands associated with insoluble complexes	
			λ (nm) (A %)							
Free Que	Ethanol		254 (38)	297 (15)	345 (24)	379 (23)				
	Water (pH = 5)		255 (42)	320 (14)		378 (44)				
Quercetin complexes	Aqueous solution	Zn	252 (34)	290 (39)	320 (56)		435[a]		437 (3)	
		Co	250 (46)	288 (25)	320 (24)			499 (4)	429 (2)	486 (1)
		Ni	249 (25)	290 (17)	319 (25)		447 (33)		437 (1)	
		Cr		279 (54)	334 (7)	359 (36)		585 (3)	448 (5)	
		Mn	244 (49)	290 (18)	311 (32)		415 (2)			
Free Lut	Ethanol		253 (1)		315 (6)	357 (2)				
	Water (pH = 5)		256 (25)	268 (4)		346 (71)				
Luteolin complexes	Aqueous solution	Zn				355 (95)	398 (2)	550 (3)	417 (3)	
		Co	286 (82)				425 (18)		430 (2)	495 (22)
		Ni		284 (83)			428 (17)		401 (13)	
		Cr	235 (61)			361 (37)		551 (2)	428 (2)	
		Mn	250 (47)		327 (52)		451 (1)		425 (2)	

[a] Detectable, but it cannot be deconvoluted.

band at longer wavelengths, typically exceeding 400 nm (Fig. 2c and Fig. S5†). Moreover, a blue-shift of the band at 290 nm can be detected with an overall increase in the absorbance of band (II). Such spectral features suggest the involvement of the entire π-conjugated system of quercetin upon complexation with the metal cation, but especially the electronic structure of rings B and C, mainly contributing to the band (I).[23,29,36]

In previous studies conducted in organic solvents or mixed organic/aqueous solvents, complexation at the 3,4-site with various metal cations (*e.g.*, Al(III), Mo(IV), Co(II), and rare earth metals) is preferred at acidic pH and at relatively low metal-to-ligand mole ratios.[29] The associated electronic absorption spectrum exhibits a band at about 425 nm, originating from the pyronium structure with a contribution of the cinnamoyl and benzoyl resonant structures involving the 3′-OH and 7-OH groups, respectively.[29] In contrast, most of these studies do agree with a preferred catechol binding complexation mode at alkaline pH (and relatively high metal-to-ligand mole ratio), featured by a band occurring at longer wavelengths (440–700 nm) in the absorption spectrum. Recently, similar results were reported for the Fe(II)- and Fe(III)-Que complexes in methanol/water, highlighting that the low-energy bands occurring at *ca.* 430 nm and at wavelengths between 500–800 nm (broad) originate from ligand to metal charge transfer transitions (LMCT) for the metal-3-hydroxychromone binding and the metal-catechol binding, respectively.[22] A LMCT mechanism was also proposed to identify complex formation in pure water between Que and various metal ions.[34] At pH 4, complexes were detected with Cr(III), Fe(III), Co(II), Cu(II), and Al(III), while at pH 7.4, complexes formed with Cr(III), Fe(III), Co(II), Ni(II), Cu(II), and Al(III). However, no complexes were observed with Mn(II), Ni(II), or Zn(II) at pH 4, in agreement with this work (Table 2 and Fig. S1†) and,[33] nor with Zn (II) at pH 7.4, in contrast to this work (Table 2 and Fig. S1†).[34]

The UV-Vis spectra of luteolin complexes showed similar features (Fig. 2d and Fig. S5†) as those of the quercetin ones, with the bleaching (Co and Ni) or partial bleaching/blue shift (Cr, Zn and Mn) of the cinnamoyl band and the formation of new low-intensity bands above 425 nm (Table 2, Fig. S5 and Table S8†). Specifically, there was a low intensity absorption between 400–460 nm in the complex-associated spectra of Lut with Ni and Mn and a wide absorption for $\lambda > 550$ nm in the other luteolin-metal complexes (Table 2). These observations do not fully align with previous data in pure water at 37 °C, where no complexes were detected with Mn(II), Fe(III), Ni(II), Cu(II) and Zn(II) at pH 4 and with Cr(III), Mn(II), Co(II), Cu(II) and Zn(II) at pH 7.4.[34]

Fig. 2e and f shows the spectra of the ethanolic solutions obtained by dissolving the solids precipitated during titrations, which can be associated with the formation of neutral complexes (Table 1). The predominant spectral features are characteristic of the free ligands, with additional high-wavelength bands above 400 nm that mainly indicate HOMO–LUMO intra-ligand transitions of the complexes (Fig. S6, Tables S9 and S10†). These spectra clearly arise from a superposition between those of the free ligands and of the complexes. This is because the titrations were carried out in saturated aqueous solutions of the ligands. Therefore, the recovered solids are mixtures of the free ligand and of the insoluble complexes. Interestingly, all of the insoluble complexes exhibit a characteristic band below 450 nm, which is close to that found in the spectra of the soluble complexes (Table 2). However, an additional band was found at longer wavelengths for Co, characterizing the spectra of the soluble complexes, although it peaked at a different wavelength. Comparing these results with those reported previously on the ethanol soluble fraction,[34] we note that while they almost align for Que, they do not for Lut, since only the complex with Mn(II) was detected at pH 7.4.[34]

In agreement with the experimental observations (Fig. 2) and literature data, the simulated UV-Vis absorption spectra (Fig. S7 and S8†) of the most stable complexes (Fig. 1), reveal that coordination with any metal and at any of the available sites on both ligands results in significant spectral changes. Specifically, the spectra of the complexes are characterized by the bleaching or partial bleaching of band I and at least one absorption band significantly red-shifted compared to band I of the free ligands (excluding the systematic underestimation of absorption band energies) (Fig. S7 and S8†). Interestingly, the most distinctive features resulting from the DFT analysis is that coordination at the 3,4 site of quercetin, induces a greater red shift compared to the 4,5 site (Fig. S7†). In contrast, coordination of Ni(II) and Mn(II) at the 3′,4′ and 4,5 sites of luteolin (Lut) produces red-shifted bands of comparable energy (Fig. S8†). Additionally, the extent of the spectral changes is clearly influenced by the type of metal cation, as demonstrated by the unique behaviour of chromium in quercetin complexes.

The complexity of the observed spectral features reflects the distribution of various species in the titration mixtures (Table 1 and Fig. S1†) that could involve different binding sites, as the binding selectivity is generally less than 100% for a specific site (Table 1).

3.4 FT-IR analysis

The involvement of the carbonyl group and the C ring in complex formation is shown through the FT-IR investigation on the solids formed during the potentiometric titration. In the FT-IR spectra (Table 3 and Fig. S9†), several key diagnostic peaks were observed.[22,31,52] These include the stretching vibrations of the carbonyl (C=O) and aromatic C=C bonds, the symmetric and asymmetric stretching of C–O–C bonds, as well as the stretching and bending vibrations of the C–C(=O)–C bonds in the C ring and the C–OH groups, along with the O–H stretching vibration.[22,31,52,53] The formation of metal–ligand complexes in aqueous solution is supported by the presence of a characteristic metal-to-ligand charge transfer band in the IR spectra at 632 nm.[22,31,52,53] However, this peak is absent in Cr-Que and Cr-Lut complexes, likely due to the presence of a mixture of complexes and unreacted free ligand, with the latter being the predominant fraction. In the IR spectra of Ni-/Co-/

Table 3 IR data (cm^{-1}) for quercetin, luteolin and corresponding complexes

		ν (O–H)	ν (C═O)	ν (C═C)	ν (C–OH)	ν (C–O–C)	ν (C–C(═O)–C)	ν (M–O)
	Quercetin	3410–3290	1666	1612, 1558, 1520	1319	1011	1165	
Quercetin complexes	Zn	3700–3200	1635	1620, 1566, 1520	—	1100	1141	632
	Co	3700–3200	1635	1620, 1566, 1520	1319 small	1100	1141	632
	Ni	3700–3200	1635 and 1705	1620, 1558, 1520	1319 small	1100	1141	632
	Cr	3700–3200	1666	1612, 1558, 1520	1319	1011	1165	—
	Mn	3700–3200	1635	1620, 1566, 1520	—	1100	1141	633
	Luteolin	3420–3280	1658	1612, 1584, 1504	1365	1033	1165	
Luteolin complexes	Zn	3700–3230	1635	1620	1365 small	—	1149	632
	Co	3700–3230	1635	1620	—	—	1149	632
	Ni	3700–3230	1635	1620	1365 small	—	1149	632
	Cr	3700–3230	1713, 1651	1612, 1584, 1504	1365	1033	1165	—
	Mn	3700–3230	1635	1620	—	—	1149	633

Zn-/Mn-Que complexes, the O–H stretching signals of the free ligand (at 3406 and 3283 cm^{-1}) extend to 3700 cm^{-1}, indicating the presence of intramolecular hydrogen bonding.

The in-plane C–OH bending at 1319 cm^{-1} is either absent or significantly attenuated. Additionally, the C═O stretching vibration shifts from 1666 cm^{-1} to 1635 cm^{-1}, suggesting a weakening of this bond and its double-bond character. A new band appears at 1705 cm^{-1} in the Ni complex. The original C═C aromatic ring stretching vibrations at 1612 cm^{-1} and 1558 cm^{-1} in free quercetin shift to 1620 cm^{-1} and 1566 cm^{-1} in Zn-/Co-/Mn-Que, while remaining unchanged in Ni-Que. In contrast, the 1520 cm^{-1} C═C band remains the same in all complexes. A strong band at 1100 cm^{-1} in the complexes is attributed to the C–O–C symmetric stretching, which appears at 1011 cm^{-1} in free quercetin. The high-energy shift in the C═C and C–O–C signals suggests increased conjugation in the C ring and enhanced molecular rigidity. Additionally, the C–C(═O)–C signal at 1165 cm^{-1} in free quercetin shifts to 1141 cm^{-1} in all complexes, with a significant increase in intensity. Similar spectral trends are observed in luteolin complexes, as summarized in Table 3 and Fig. S9.†

4 Conclusions

This study provides the first systematic evaluation of quercetin and luteolin complexation with first-row transition metals in a purely aqueous environment, shedding light on their coordination preferences and stability. Potentiometric, spectroscopic, and computational analyses collectively demonstrated that complex formation depends on metal identity, ligand structure, and pH conditions. While all the investigated metals formed stable complexes with both ligands, the overall stability was higher for quercetin due to its additional hydroxyl group, which enhances metal-binding affinity. In quercetin, binding site selectivity depends on the metal type and complex stoichiometry. Generally, the 4,5 site is preferred when the metal's coordination sphere includes water and quercetin, while the 3,4 site is favored when a hydroxyl group is present in the coordination sphere. In luteolin, the 4,5 site is always preferred, with selectivity percentages ranging from 89% to 100%. Therefore, the catechol site is always disfavored in water for both ligands, except for Fe(III).

The findings support the role of flavonoids as effective metal chelators and underscore their potential applications in antioxidant mechanisms, heavy metal sequestration, and environmental remediation. The synergy between experimental and theoretical approaches provided a comprehensive understanding of flavonoid–metal interactions, laying the groundwork for further studies on their biological and technological applications.

Author contributions

Giuseppina Anna Corrente: investigation, validation, and formal analysis. Luana Malacaria: investigation and validation. Amerigo Beneduci: conceptualization, methodology, formal analysis, validation, writing – original draft, writing – review & editing, supervision, and funding acquisition. Tiziana Marino: conceptualization, methodology, writing – original draft, writing – review & editing, and funding acquisition. Emilia Furia: conceptualization, methodology, writing – original draft, writing – review & editing, and funding acquisition.

Data availability

The authors declare that the data supporting the findings of this study are available within the article and its ESI.† Additional data are available from the corresponding authors upon reasonable request.

Conflicts of interest

The authors declare that they have no competing interest.

Acknowledgements

The authors thank the Dipartimento di Chimica e Tecnologie Chimiche, Università della Calabria, for the financial support through funding MUR EX60%.

References

1 A. Zeb, *Phenolic Antioxidants in Foods: Chemistry, Biochemistry and Analysis*, Springer International Publishing, Cham, 2021.
2 S. Chen, X. Wang, Y. Cheng, H. Gao and X. Chen, *Molecules*, 2023, **28**, 4982.
3 A. Seyoum, K. Asres and F. K. El-Fiky, *Phytochemistry*, 2006, **67**, 2058–2070.
4 L. Malacaria, R. Bruno, G. A. Corrente, D. Armentano, E. Furia and A. Beneduci, *J. Mol. Liq.*, 2022, **346**, 118302.
5 E. Rodríguez-Arce and M. Saldías, *Biomed. Pharmacother.*, 2021, **143**, 112236.
6 H. Sigel and A. Sigel, *Z. Naturforsch., B:J. Chem. Sci.*, 2019, **74**, 461–471.
7 C. Van Cleave and D. C. Crans, *Inorganics*, 2019, **7**, 111.
8 L. Marchiò, N. Marchetti, C. Atzeri, V. Borghesani, M. Remelli and M. Tegoni, *Dalton Trans.*, 2015, **44**, 3237–3250.
9 T. D. Rae, P. J. Schmidt, R. A. Pufahl, V. C. Culotta and T. V. O'Halloran, *Science*, 1999, **284**, 805–808.
10 T. Kiss, É.A Enyedy and T. Jakusch, *Coord. Chem. Rev.*, 2017, **352**, 401–423.
11 A. Levina, D. C. Crans and P. A. Lay, *Coord. Chem. Rev.*, 2017, **352**, 473–498.
12 M. Valko, H. Morris and M. T. D. Cronin, *Curr. Med. Chem.*, 2005, **12**, 1161–1208.
13 H. Dong, X. Yang, J. He, S. Cai, K. Xiao and L. Zhu, *RSC Adv.*, 2017, **7**, 53385–53395.
14 D. C. Crans and K. Kostenkova, *Commun. Chem.*, 2020, **3**, 1–4.
15 G. J. Kontoghiorghes, *Int. J. Mol. Sci.*, 2020, **21**, 2499.
16 J.-J. Kim, Y.-S. Kim and V. Kumar, *J. Trace Elem. Med. Biol.*, 2019, **54**, 226–231.
17 G. J. Kontoghiorghes and C. N. Kontoghiorghe, *Expert Opin. Invest. Drugs*, 2019, **28**, 593–603.
18 V. S. Fedenko, M. Landi and S. A. Shemet, *Int. J. Mol. Sci.*, 2022, **23**, 11370.
19 S. Manikandan, D. Inbakandan, C. Valli Nachiyar and S. Karthick Raja Namasivayam, *Sustain. Chem. Environ.*, 2023, **2**, 100001.
20 D. Dutta, R. Rautela, L. K. S. Gujjala, D. Kundu, P. Sharma, M. Tembhare and S. Kumar, *Sci. Total Environ.*, 2023, **859**, 160391.
21 P. R. Jadhao, E. Ahmad, K. K. Pant and K. D. P. Nigam, *Sep. Purif. Technol.*, 2022, **289**, 120773.
22 W. Xu, S. Pan, B. B. Noble, J. Chen, Z. Lin, Y. Han, J. Zhou, J. J. Richardson, I. Yarovsky and F. Caruso, *Angew. Chem., Int. Ed.*, 2022, **61**, e202208037.
23 H. Ejima, J. J. Richardson and F. Caruso, *Nano Today*, 2017, **12**, 136–148.
24 R. F. V. de Souza and W. F. De Giovani, *Spectrochim. Acta, Part A*, 2005, **61**, 1985–1990.
25 M. M. Kasprzak, A. Erxleben and J. Ochocki, *RSC Adv.*, 2015, **5**, 45853–45877.
26 A.-H. Yang, X.-Y. Shi, X. Li, F.-F. Li, Q.-Q. Zhang, S.-X. Jiang, J.-Z. Cui and H. Gao, *RSC Adv.*, 2014, **4**, 25227–25233.
27 H. E. Hajji, E. Nkhili, V. Tomao and O. Dangles, *Free Radical Res.*, 2006, **40**, 303–320.
28 A. Pękal, M. Biesaga and K. Pyrzynska, *BioMetals*, 2011, **24**, 41–49.
29 J. P. Cornard and J. C. Merlin, *J. Inorg. Biochem.*, 2002, **92**, 19–27.
30 A. Primikyri, G. Mazzone, C. Lekka, A. G. Tzakos, N. Russo and I. P. Gerothanassis, *J. Phys. Chem. B*, 2015, **119**, 83–95.
31 S. B. Bukhari, S. Memon, M. Mahroof-Tahir and M. I. Bhanger, *Spectrochim. Acta, Part A*, 2009, **71**, 1901–1906.
32 L. Malacaria, G. A. Corrente, A. Beneduci, E. Furia, T. Marino and G. Mazzone, *Molecules*, 2021, **26**, 2603.
33 G. A. Corrente, L. Malacaria, A. Beneduci, E. Furia, T. Marino and G. Mazzone, *J. Mol. Liq.*, 2021, **325**, 115171.
34 L. Malacaria, J. Bijlsma, R. Hilgers, W. J. C. De Bruijn, J.-P. Vincken and E. Furia, *J. Mol. Liq.*, 2023, **369**, 120840.
35 E. Furia and R. Porto, *J. Chem. Eng. Data*, 2008, **53**, 2739–2745.
36 E. Vasca, S. Materazzi, T. Caruso, O. Milano, C. Fontanella and C. Manfredi, *Anal. Bioanal. Chem.*, 2002, **374**, 173–178.
37 K. Emerson and W. M. Graven, *J. Inorg. Nucl. Chem.*, 1959, **11**, 309–313.
38 E. Furia, D. Aiello, L. D. Donna, F. Mazzotti, A. Tagarelli, H. Thangavel, A. Napoli and G. Sindona, *Dalton Trans.*, 2013, **43**, 1055–1062.
39 L. Malacaria, G. A. Corrente and E. Furia, *Appl. Sci.*, 2021, **11**, 4475.
40 M. H. Abraham and W. E. Acree, *J. Mol. Liq.*, 2014, **197**, 157–159.
41 S. Rajhard, L. Hladnik, F. A. Vicente, S. Srčič, M. Grilc and B. Likozar, *Processes*, 2021, **9**, 1952.
42 G. Biedermann and L. G. Sillén, *Ark. Kemi*, 1953, 425–440.
43 P. Gans, A. Sabatini and A. Vacca, *J. Chem. Soc., Dalton Trans.*, 1985, 1195–1200.
44 L. G. Sillén, S. G. Terjesen, R. A. Cox and A. R. Peacocke, *Acta Chem. Scand.*, 1956, **10**, 803–811.
45 M. J. Frisch, G. W. Trucks, *et al.*, *Gaussian 16, rev. C.01*, Gaussian, Inc., Wallingford, CT, 2016.
46 A. V. Marenich, C. J. Cramer and D. G. Truhlar, *J. Phys. Chem. B*, 2009, **113**, 6378–6396.
47 R. F. Ribeiro, A. V. Marenich, C. J. Cramer and D. G. Truhlar, *J. Phys. Chem. B*, 2011, **115**, 14556–14562.
48 L. Skripnikov, Chemissian Version 4.43, Visualization Computer Program **https://www.chemissian.com**, 2016.
49 E. H. Anouar, J. Gierschner, J.-L. Duroux and P. Trouillas, *Food Chem.*, 2012, **131**, 79–89.
50 A. Primikyri, G. Mazzone, C. Lekka, A. G. Tzakos, N. Russo and I. P. Gerothanassis, *J. Phys. Chem. B*, 2015, **119**, 83–95.
51 L.-G. Gao, H. Wang, X.-L. Song and W. Cao, *J. Mol. Struct.*, 2013, **1034**, 386–391.
52 R. F. V. de Souza and W. F. De Giovani, *Spectrochim. Acta, Part A*, 2005, **61**, 1985–1990.
53 A.-H. Yang, X.-Y. Shi, X. Li, F.-F. Li, Q.-Q. Zhang, S.-X. Jiang, J.-Z. Cui and H. Gao, *RSC Adv.*, 2014, **4**, 25227–25233.